

Projections of Hydroclimatic Extremes in Southeast Alaska under the RCP8.5 Scenario

RICK LADER,^a UMA S. BHATT,^{a,b} JOHN E. WALSH,^a AND PETER A. BIENIEK^a

^a International Arctic Research Center, University of Alaska Fairbanks, Fairbanks, Alaska

^b Geophysical Institute, University of Alaska Fairbanks, Fairbanks, Alaska

(Manuscript received 23 November 2021, in final form 8 June 2022)

ABSTRACT: Parts of southeast Alaska experienced record drought in 2019, followed by record daily precipitation in late 2020 with substantial impacts to human health and safety, energy resources, and fisheries. To help ascertain whether these types of events can be expected more frequently, this study investigated observed trends and projected changes of hydroclimatic extremes indices across southeast Alaska, including measures of precipitation variability, seasonality, magnitude, and type. Observations indicated mixed tendencies of interannual precipitation variability, but there were consistent trends toward warmer and wetter conditions. Projected changes were assessed using dynamically downscaled climate model simulations at 4-km spatial resolution from 2031 to 2060 that were compared with a historical period from 1981 to 2010 using two models—NCAR CCSM4 and GFDL CM3. Consistent directional changes were found for five of the analyzed indices. The CCSM indicated increased maximum 1-day precipitation (RX1; 12.6%), increased maximum consecutive 5-day precipitation (RX5; 7.4%), longer periods of consecutive dry days (CDD; 11.9%), fewer snow cover days (SNC; -21.4%) and lower snow fraction (SNF; -24.4%); for GFDL these changes were 19.8% for RX1, 16.0% for RX5, 20.1% for CDD, -21.9% for SNC, and -26.5% for SNF. Although both models indicated substantial snow losses, they also projected annual snowfall increases at high elevations; this occurred above 1500 m for CCSM and above 2500 m for GFDL. Significance testing was assessed at the 95% confidence level using Theil–Sen's slope estimates for the observed time series and the Wilcoxon–Mann–Whitney *U* test for projected changes of the hydroclimatic extremes indices relative to their historical distributions.

KEYWORDS: Drought; Extreme events; Flood events; Downscaling

1. Introduction

Southeast Alaska faced exceptional variability of hydroclimatic extremes between the summer of 2019 and autumn 2020, beginning with record-breaking drought (Thoman and Walsh 2019) and ending with flooding rains that triggered mudslides, avalanches, and loss of life (Anchorage Daily News 2020). Data from the Global Historical Climatology Network–Daily database (GHCN-D; Menne et al. 2012) show that single-day precipitation records were set on 1 December 2020 at Juneau (12.5 cm), Haines (13.9 cm), and Skagway (9.3 cm). These events came on the heels of a multiyear drought that peaked in 2019, which prompted the region's first extreme drought classification (D3, per the U.S. Drought Monitor; National Drought Mitigation Center 2021). Bathke et al. (2019) concluded that this drought impacted various human and ecological sectors, including fisheries (harmful algal blooms and species mortality), water supply (decreased municipal availability and hydropower production), and communities (increased energy costs and air pollution from diesel power generation).

It is not uncommon for extreme precipitation events to follow drought. The flooding of December 2020 was attributed to an atmospheric river (AR), or a plume of subtropical moisture that was transported to the extratropics. These ARs have often

been considered “drought breakers,” and Dettinger (2013) found that the majority of droughts in the Pacific Northwest (60%–74%) from 1950 to 2010 were broken by ARs. Despite the possibility that this dry-to-wet pattern could lead to near-normal precipitation amounts over a long period, there are consequences as compared with more regularly spaced precipitation. Extended dry periods reduce the structural integrity of soil, which then makes it prone to scour, erosion, and subsidence under heavy precipitation (Vahedifard et al. 2016); desiccated soil is also less able to absorb water, which means that precipitation will runoff quickly and be lost.

Average annual precipitation has been increasing across southeast Alaska. From 1969 to 2018, each of the four Alaska climate divisions from this region (NOAA NCEI 2015) showed increased precipitation amounts that ranged from 4.7% in the South Panhandle up to 15.1% in the Central Panhandle (Thoman and Walsh 2019). The region-averaged annual precipitation from 1981 to 2010 was 312 cm (Lader et al. 2020) and Sharma and Déry (2020) found that ARs contributed up to 33% of annual precipitation and up to 97% of seasonal extreme amounts from 1979 to 2012. Easterling et al. (2017) found that 99th percentile precipitation increased by 16% Alaska statewide from 1958 to 2016. Current projections for Alaska indicated increased hydroclimate variability, such that extreme precipitation events will continue to produce higher amounts (Walsh et al. 2014). In the western United States, ARs are expected to account for a higher percentage of total precipitation, with more dry days and fewer low-to-moderate precipitation events (Gershunov et al. 2019).

The IPCC defined disaster risk as the combined effects of vulnerability, exposure, and weather and climate events

Corresponding author: Rick Lader, rtladerjr@alaska.edu

Earth Interactions is published jointly by the American Meteorological Society, the American Geophysical Union, and the Association of American Geographers.

DOI: 10.1175/EI-D-21-0023.1

© 2022 American Meteorological Society. For information regarding reuse of this content and general copyright information, consult the AMS Copyright Policy (www.ametsoc.org/PUBSReuseLicenses).

(IPCC 2012). Southeast Alaska, which is an area covered primarily with coastal rain forest, expansive high-elevation ice fields and steep topographical gradients, presents unique challenges because of its geography and remoteness. Most of the region is only accessible by air or sea—including the state capital, Juneau—meaning that there is a lack of redundancy that is typically built into essential networks; for example, if the single access road between the Juneau Airport and downtown is compromised due to flooding or an avalanche, then the community is at heightened risk. There is also a dependence on hydropower and dam operation for basic energy and water services, and these sectors are at risk due to changing precipitation patterns (EPA 2017). For example, snow as a fraction of total precipitation has been decreasing in the western United States (Knowles et al. 2006; Wehner et al. 2017) and, as a result of earlier snowmelt, peak runoff shifted more than 10 days earlier in the spring from 1948 to 2002 in southeast Alaska (Dettinger 2005; Stewart 2009). Beyond the implications of predictability for hydropower operations, communities depend on seasonal snowmelt for drinking water and the regulation of streamflow and stream temperature, which with less snow and higher temperatures can become low, warm, and oxygen poor, thus impacting seasonal salmon migration.

This study has three primary objectives, which are to assess historical and projected

- 1) interannual precipitation variability in terms of magnitude and spell duration,
- 2) extreme precipitation events and their seasonality, and
- 3) changes in snow cover, snow fraction, and their topographical nature across southeast Alaska.

Section 2 of this paper explains the data and methods used, including a description of observational data, model simulations, trend analysis, and climate extreme indices. Section 3 describes the results, which are broken down into observed trends, followed

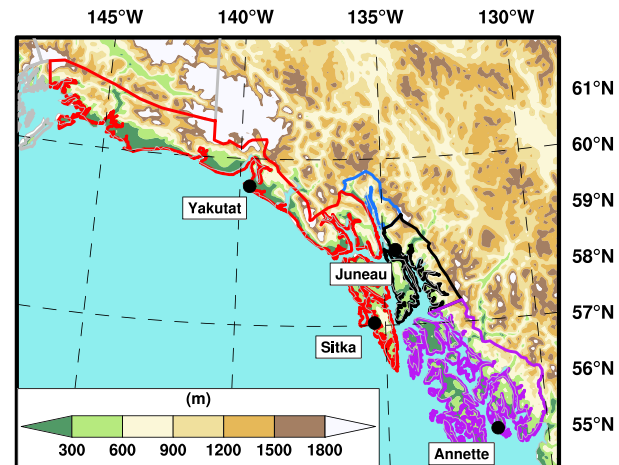


FIG. 1. Study domain and model terrain height (m) showing station locations and Alaska climate divisions, including the Northeast Gulf (red), North Panhandle (blue), Central Panhandle (black), and South Panhandle (purple).

by historical and projected precipitation and snowfall indices. A discussion of these results follows in section 4, prior to concluding remarks in section 5.

2. Data and methods

a. Data

1) STATION-BASED TEMPERATURE, PRECIPITATION, AND SNOW DEPTH OBSERVATIONS

Monthly temperature and precipitation were retrieved from the NOAA NCEI Climate at a Glance tool, covering the period from 1925 to 2020 for four climate divisions across southeast Alaska (<https://www.ncdc.noaa.gov/cag/>; NOAA

TABLE 1. Mean and trend statistics of 2-m temperature (T2) and precipitation (PCPT) from observations (i.e., NOAA NCEI) and model results by climate division and aggregated for all of southeast Alaska. Significant changes at 95% confidence are in boldface font.

Climate division	Obs (1925–2020) mean (°C or cm)		Obs (1925–2020) trend (°C or cm decade ⁻¹)	Historical period (1981–2010) obs and modeled mean (°C or cm)				Projected (2031–60) change in mean (±°C or ±%)	
	NCEI			NCEI	CFSR	CCSM	GFDL	CCSM	GFDL
T2									
Northeast Gulf	0.7		0.1	1.1	0.8	0.6	-0.2	+1.8	+2.4
North Panhandle	0.2		0.0	0.3	0.1	0.3	-0.9	+1.8	+2.4
Central Panhandle	1.8		0.1	2.1	2.1	2.3	1.5	+1.8	+2.3
South Panhandle	4.7		0.1	5.0	4.5	4.7	4.3	+1.8	+2.2
Southeast Alaska	2.0		0.1	2.3	2.0	2.0	1.3	+1.8	+2.3
Precipitation									
Northeast Gulf	418.1		-4.6	422.7	327.2	383.6	405.4	+7.4	+1.8
North Panhandle	217.0		-1.3	214.4	216.8	224.0	254.5	+3.9	+1.1
Central Panhandle	417.7		3.9	437.9	317.5	341.7	357.9	+4.2	+3.2
South Panhandle	362.1		1.4	368.7	298.7	287.9	300.0	+4.6	+7.4
Southeast Alaska	391.8		-1.8	398.6	312.3	342.4	361.0	+6.2	+3.3

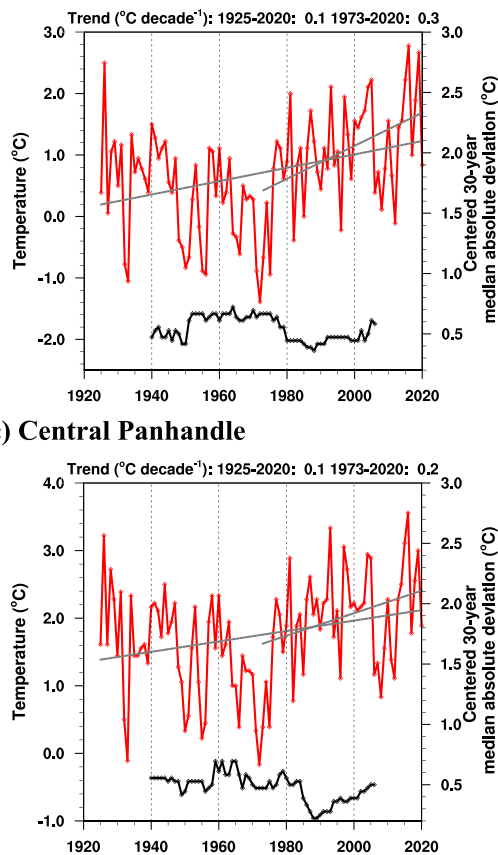
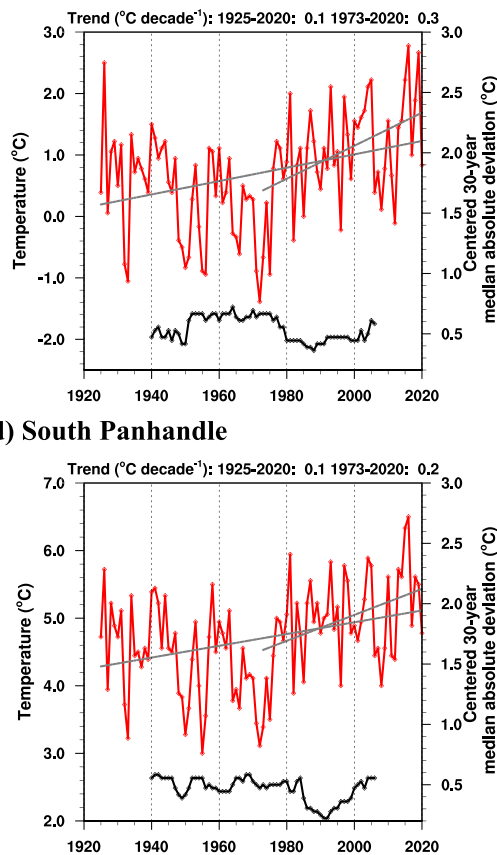
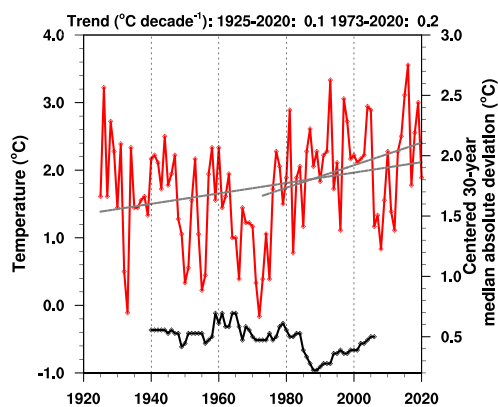
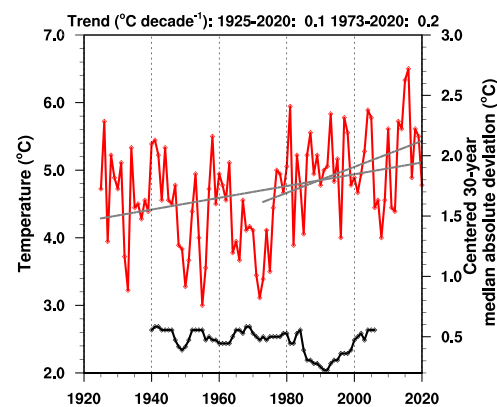
a) Northeast Gulf**b) North Panhandle****c) Central Panhandle****d) South Panhandle**

FIG. 2. Time series of 2-m temperature (red; $^{\circ}\text{C}$) from NOAA NCEI for the Alaska climate divisions of (a) Northeast Gulf, (b) North Panhandle, (c) Central Panhandle, and (d) South Panhandle. Theil-Sen trends of the full period of record (1925–2020) and the most recent half (1973–2020) are shown in gray, with the values above each plot. The centered 30-yr median absolute deviation (black) is shown by the y axis on the right of each plot, with each symbol corresponding to the 30-yr period centered in the year marked (i.e., the first symbol measured the 1925–54 period).

NCEI 2021). These divisions are shown in Fig. 1 and include the Northeast Gulf, North Panhandle, Central Panhandle, and South Panhandle. The monthly values were derived from daily station data, as available, and the divisions were originally developed based on regions with similar climate variability and airmass characteristics (Bieniek et al. 2012). A map of stations included in these products is available in Vose et al. (2017).

Daily observations of snow depth were retrieved from the GHCN-D database (Menne et al. 2012) from four stations in Alaska. These four stations, with their location and years of suitable coverage included Yakutat (59.50°N , 139.66°W ; 1949–2017), Juneau (58.36°N , 134.58°W ; 1949–2020), Sitka (57.05°N , 135.25°W ; 1948–96), and Annette (55.04°N , 131.57°W ; 1942–2017). Years were included for analysis if data coverage was at least 95% for a given year; this essentially restricted the list of usable stations to these four and demonstrates the lack of long-term observations available for climate study in this region. The snow depth variable was used to calculate annual days with snow cover, which assumed a minimum depth of 2.54 cm (1.0 in.).

2) DYNAMICALLY DOWNSCALED REANALYSIS AND CLIMATE MODEL SIMULATIONS

This study used dynamically downscaled reanalysis and climate model simulations to better understand historical (1981–2010) and projected (2031–60) hydroclimatic extremes across southeast Alaska. All simulations were downscaled to $4\text{ km latitude} \times 4\text{ km longitude}$ spatial resolution using the Weather Research and Forecasting (WRF) Model, version 4 (Skamarock et al. 2019). The Climate Forecast System Reanalysis (CFSR; Saha et al. 2010), originally at $\sim 38\text{-km}$ spatial resolution, served as the reanalysis forcing for the 1981–2010 period. The CFSR was selected for its overall forecasting performance among seven reanalysis models in northern latitudes (Lindsay et al. 2014) and more specifically for its consistency with independent precipitation observations in southeast Alaska (Lader et al. 2016). Simulations for the historical and future periods (through 2060) were obtained by downscaling two global climate models—the National Center for Atmospheric Research Community Climate System Model, version 4 (CCSM; $1.25^{\circ} \times 0.9^{\circ}$; Gent et al. 2011), and the NOAA Geophysical Fluid Dynamics Laboratory Climate Model, version

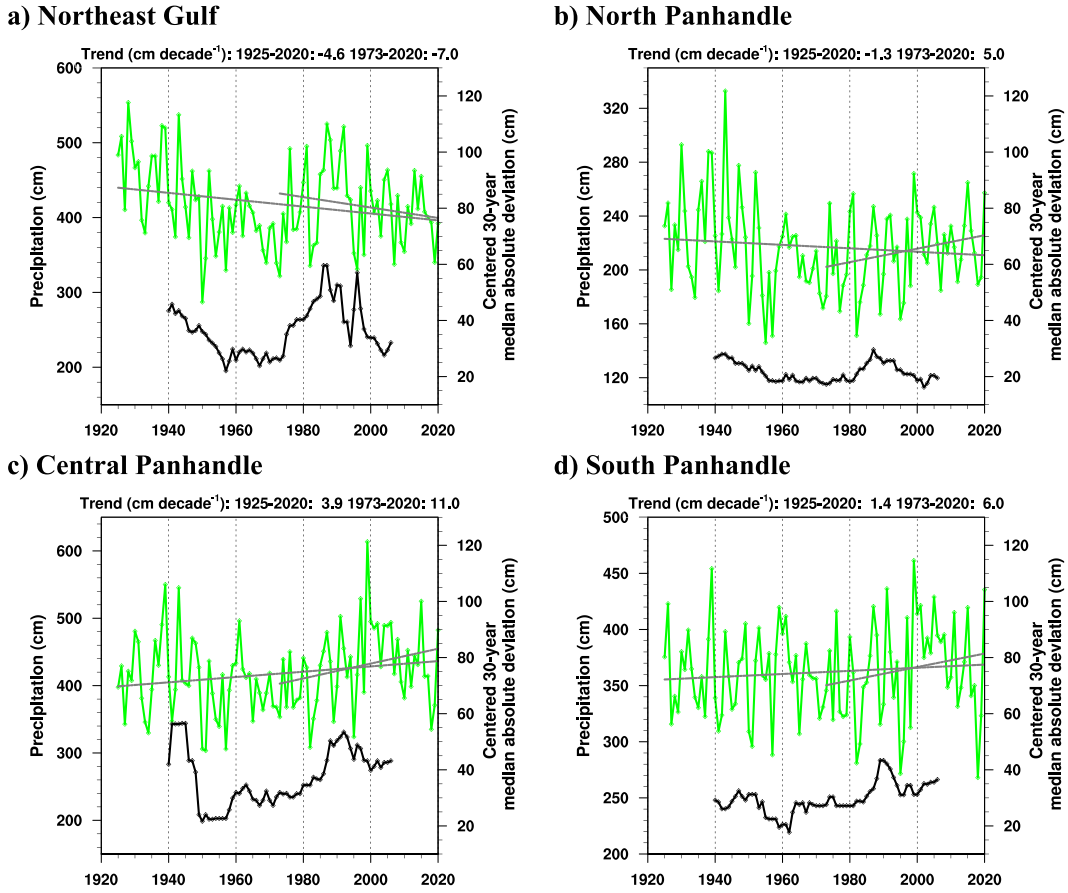


FIG. 3. As in Fig. 2, but for precipitation (green; cm).

3 (GFDL; ~200-km cubed sphere; Donner et al. 2011). The downscaled data were obtained from the Scenarios Network for Alaska and Arctic Planning and are available online (<https://registry.opendata.aws/wrf-se-alaska-snap/>). The climate model forcing runs for the projected periods came from representative concentration pathway 8.5 (RCP8.5; Riahi et al. 2011) from phase 5 of the Coupled Model Intercomparison Project (Taylor et al. 2012). Because RCP8.5 is at the upper end of the range of radiative forcing spanned by the RCP emission scenarios, it offers the greatest potential for signal detection in high-latitude hydrology. Other RCP scenarios will generally provide more muted responses to anthropogenic forcing.

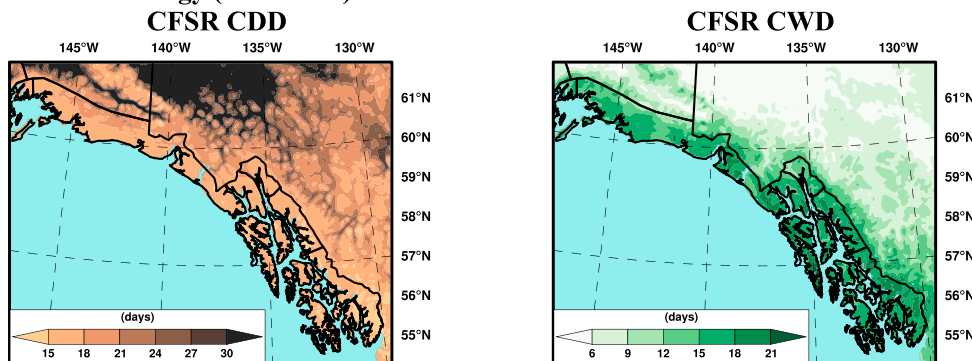
Each 30-yr simulation was a continuous run with 6-hourly nudging from the forcing data and was preceded by a 17-month model spinup period to properly initialize the land surface state. Cumulus parameterization in the WRF was turned off because a 4-km spatial resolution is considered to be convection permitting (Prein et al. 2015). The key physics parameters used, with their WRF option name in parentheses, included microphysics (Thompson; Thompson et al. 2008), longwave and shortwave radiation (Rapid Radiative Transfer Model; Iacono et al. 2008), planetary boundary layer (Yonsei University; Hong et al. 2006), surface layer (MM5 similarity; Jiménez et al. 2012), lake (WRF-Lake; Gu et al. 2015; Subin et al. 2012), and surface (Noah-MP land surface model; Niu

et al. 2011). More information on the parameterization schemes used is shown in Table 1 of Lader et al. (2020). These WRF parameterization options were also used by Monaghan et al. (2018) for downscaled simulations that covered Alaska from 2002 to 2016. Postprocessed WRF output was saved at daily and hourly time resolution and the daily data were used in this study to calculate the hydroclimatic extremes indices.

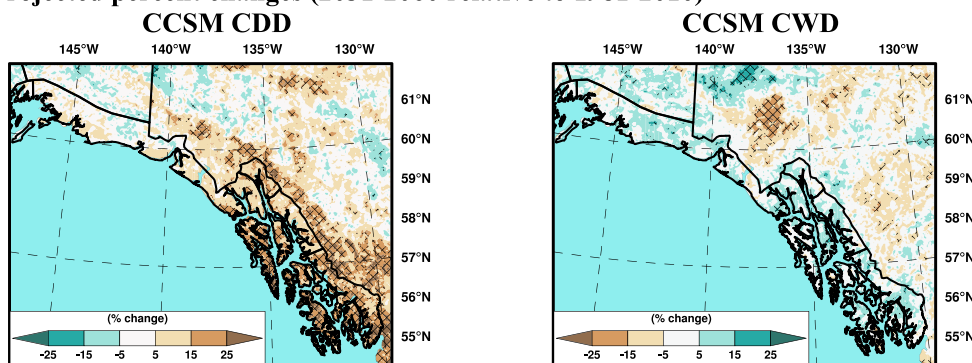
b. Methods

All trend and hydroclimate extremes index calculations were performed using NCAR Command Language (NCL, version 6.4.0; NCAR 2022) and R Statistical Software (version 4.1.3; R Core Team 2022). Stated trends in this paper were calculated using Theil–Sen's estimates of median slopes (Sen 1968; Theil 1950), which is a nonparametric technique that is less sensitive to outliers than ordinary least squares regression. Trends were considered statistically significant at and above the two-tailed 95% confidence level. The observed temperature and precipitation trends in section 3a were calculated for the full period of record (1925–2020) and the last half of this period (1973–2020) to identify both the long-term tendency and whether there has been a more recent change in sign or an amplification of the trend. Differences of extremes index values between the projected and historical periods

a) CFSR climatology (1981-2010)



b) Projected percent changes (2031-2060 relative to 1981-2010)



c) Projected percent changes (2031-2060 relative to 1981-2010)

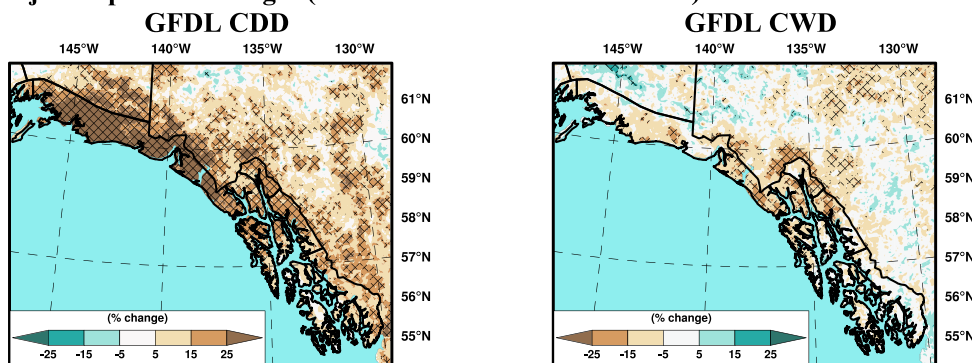


FIG. 4. (a) Climatological mean values of the annual maximum number of (left) CDD and (right) CWD from the downscaled 4-km CFSR (1981–2010) and projected percent changes (2031–60 mean relative to 1981–2010 mean) from (b) CCSM and (c) GFDL. Significant changes that met the 95% confidence level are hatched.

were tested at the 95% confidence level using the nonparametric Wilcoxon–Mann–Whitney U test (Mann and Whitney 1947), which does not assume that the two data samples follow a normal distribution.

In this study, the hydroclimatic extremes indices included annual-based values of maximum number of consecutive dry days (CDD) and consecutive wet days (CWD), maximum 1- and 5-day precipitation (RX1 and RX5, respectively), snow cover days (SNC), and snow fraction (SNF) of total precipitation. CDD and CWD identified the longest period annually with consecutive days when precipitation was below 1.0 mm, or equal to or above 1.0 mm, respectively. RX1 and RX5, both measured in centimeters, identified the single wettest day and

wettest consecutive 5-day window each year, respectively. SNC used two thresholds: one for station observations (2.54 cm) and another for model data (1.0 mm), with the former based on the minimum allowable station measurement of snow depth and the latter to be consistent with the other indices (e.g., CDD). SNF divided total snowfall, measured in liquid equivalent (cm) by total precipitation (cm).

The hydroclimatic extremes indices were based off of those introduced by Zhang et al. (2011), which were designed to facilitate cross-regional assessments of temperature and precipitation extremes. Future projections of these indices were presented as model percent changes, such that each climate model's future mean is presented relative to its historical

TABLE 2. Historical mean (1981–2010) and projected percent changes (2031–60) of annual maximum number of consecutive dry days (CDD) and wet days (CWD) and annual maximum 1-day (RX1) and 5-day (RX5) precipitation by model and climate division. Significant changes at 95% confidence are in boldface font.

Climate division	1981–2010 mean (days or cm)			2031–60 projected change (±%)	
	CFSR	CCSM	GFDL	CCSM	GFDL
Annual max no. of CDD					
Northeast Gulf	17.0	21.9	16.2	+7.2	+26.4
North Panhandle	17.2	22.4	17.5	+14.2	+18.7
Central Panhandle	15.7	20.1	15.6	+12.9	+16.6
South Panhandle	15.5	22.5	15.6	+19.1	+10.0
Southeast Alaska	16.4	21.9	16.0	+11.9	+20.1
Annual max no. of CWD					
Northeast Gulf	16.0	16.3	17.1	+3.7	-8.8
North Panhandle	14.0	14.7	15.8	+2.5	-11.3
Central Panhandle	16.5	17.6	17.4	+6.1	-7.6
South Panhandle	16.3	16.0	15.5	+2.9	-2.2
Southeast Alaska	16.0	16.3	16.6	+3.7	-7.0
Annual max RX1					
Northeast Gulf	11.3	12.7	13.2	+16.4	+21.7
North Panhandle	7.3	8.1	8.8	+9.4	+22.2
Central Panhandle	9.5	10.7	11.9	+8.7	+15.7
South Panhandle	9.3	10.8	9.8	+6.6	+17.0
Southeast Alaska	10.3	11.6	11.8	+12.6	+19.8
Annual max RX5					
Northeast Gulf	25.8	31.4	30.5	+10.1	+18.7
North Panhandle	17.0	19.5	20.2	+0.4	+15.4
Central Panhandle	22.2	26.0	27.0	+3.6	+9.9
South Panhandle	20.5	24.3	21.0	+3.6	+12.1
Southeast Alaska	23.3	28.1	26.7	+7.4	+16.0

mean. The climate models' historical means were also compared with those of the CFSR (i.e., gridded observations) to consider their initial bias. The model-based indices were calculated for each grid cell before being aggregated by climate division and for all of southeast Alaska.

3. Results

Prior to describing trends and results from the hydroclimatic extremes indices, it is useful to state how well the models' mean temperature and precipitation compared to the observed products (i.e., NOAA NCEI and the downscaled CFSR) to provide a sense of confidence in the results. Each of the explicit values that follow in this section can be found in Table 1.

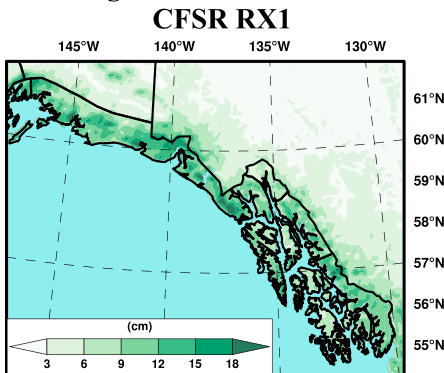
The historical CFSR temperature climatology (1981–2010) across southeast Alaska was 2.0°C, as compared with 2.3°C from the NOAA NCEI Climate at a Glance tool. The historical CCSM closely matched the observed products (2.0°C), but the GFDL was cooler at 1.3°C. On average, however, the CCSM was warmer than the CFSR in all climate divisions except the Northeast Gulf. The Northeast Gulf climate division contained 53% of the southeast Alaska land grid cells (i.e., 3825 of 7171), which helps to explain why the overall values were comparable. The GFDL was colder than the CFSR across all divisions.

The historical CFSR precipitation climatology was considerably drier (312.3 cm) than NOAA NCEI (398.6 cm). It was posited by Lader et al. (2020) that this difference was in part due to the prevalence of coastal stations, which are much wetter than inland areas, used to interpolate and produce the NOAA NCEI product. Both historical simulations from the climate models were wetter than the CFSR with southeast Alaska mean values of 342.4 and 361.0 cm in CCSM and GFDL, respectively. The CCSM was wetter than the CFSR in all climate divisions except for the South Panhandle and the GFDL was wetter in all divisions.

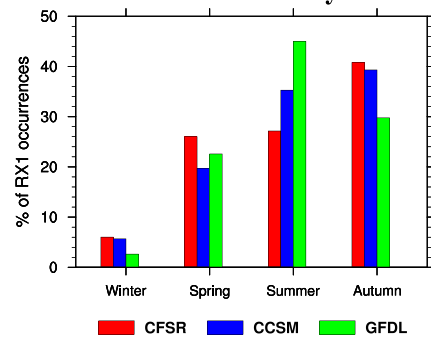
a. Observed temperature and precipitation trends

Long-term monthly temperature records (1925–2020) from the NOAA NCEI Climate at a Glance tool show significant warming in the Northeast Gulf, Central Panhandle, and South Panhandle climate divisions (Fig. 2). Notably, trends during the last half of this period, from 1973 to 2020, were substantially higher (e.g., more than double) in all four southeast Alaska climate divisions and statistically significant in all cases (Fig. 2). The largest trend during this most recent period was in the Northeast Gulf (0.3°C decade⁻¹). The centered 30-yr median absolute deviation of mean annual temperature showed similar patterns across the climate divisions, with the most notable feature being the abrupt drop in the 1980s, before rising again more recently.

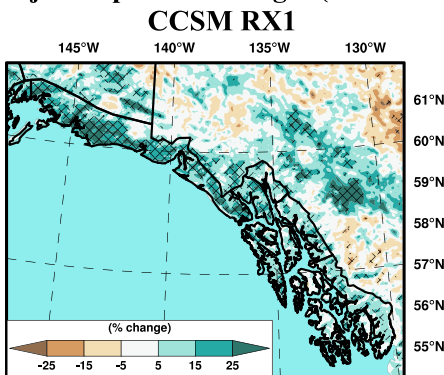
a) Climatological RX1



RX1 Seasonality



b) Projected percent changes (2031–2060 relative to 1981–2010)



GFDL RX1

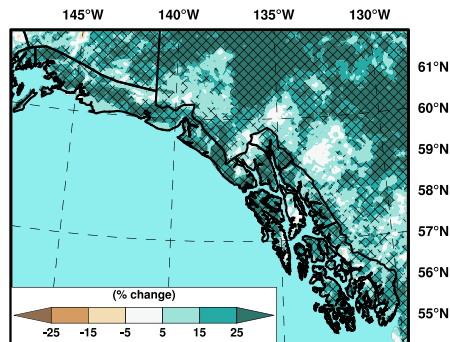


FIG. 5. (a) Downscaled 4-km climatological CFSR values of the annual RX1 (cm; left panel) and seasonal percentages of RX1 occurrence from the historical CFSR (red), CCSM (blue), and GFDL (green) (right panel); also shown are (b) projected percent changes in RX1 (2031–60 mean relative to 1981–2010 mean) from CCSM (left panel) and GFDL (right panel). Significant changes that met the 95% confidence level are hatched.

Long-term monthly precipitation records were similarly available from the NCEI Climate at a Glance tool from 1925 to 2020; however, trends were less consistent than for temperature. The Northeast Gulf had a significant decreasing trend ($-4.6 \text{ cm decade}^{-1}$; Fig. 3a) and the North Panhandle also had a decreasing trend ($-1.3 \text{ cm decade}^{-1}$; Fig. 3b). The more southerly climate divisions showed increasing trends of 3.9 and $1.4 \text{ cm decade}^{-1}$ in the Central Panhandle and South Panhandle (Figs. 3c and 3d, respectively). However, a noteworthy change was evident in the second half of this period from 1973 to 2020 when all trends, with the exception of the Northeast Gulf, became increasingly positive. The time series of centered 30-yr median absolute deviation in Fig. 3 showed a difference between the northerly regions and the southerly ones wherein recent variability was relatively low in the former and high in the latter.

b. Precipitation extremes indices

The historical CFSR climatologies of CDD and CWD are shown from left to right in Fig. 4a, with values for southeast Alaska of 16.4 and 16.0 days, respectively (see Table 2 for explicit values of these indices). The greatest divisional CDD runs were in the North Panhandle where it was typically driest. Maximum divisional CWD values were in the Central

Panhandle, which was similarly wet to the Northeast Gulf. Both historical climate model simulations had higher CWD values than CFSR, on average, across southeast Alaska, which is unsurprising given that they were both wetter. The CCSM southeast Alaska CDD climatology was substantially longer (21.9 days) than CFSR (16.4 days), but GFDL was similar (16.0 days) to CFSR.

Projected percent changes based on climatological mean values (2031–60 relative to 1981–2010) are shown for CCSM (Fig. 4b) and GFDL (Fig. 4c) for CDD and CWD from left to right. Averaged across southeast Alaska and in all four climate divisions, the models agreed on positive projected CDD change; however, the most pronounced changes in CCSM were in the southern half of the region, whereas for GFDL the northern divisions are expected to see the largest change toward longer dry periods. Signals of CWD changes were mixed among the models with CCSM suggesting longer wet periods and GFDL indicating shorter wet periods. Percent changes in CWD were considerably less in both models than were the changes toward longer dry periods.

The historical CFSR RX1 climatology is shown in Fig. 5a (right) with a southeast Alaska average of 10.3 cm, which was lower than the climate model values of 11.6 cm for CCSM and 11.8 cm for GFDL (Table 2). The most likely season for these

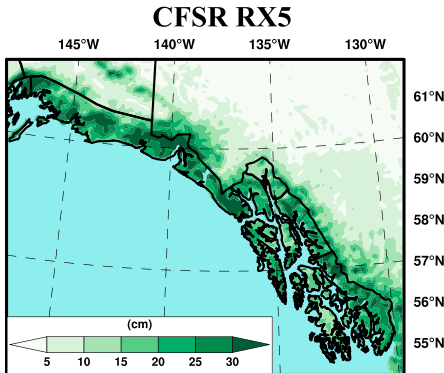
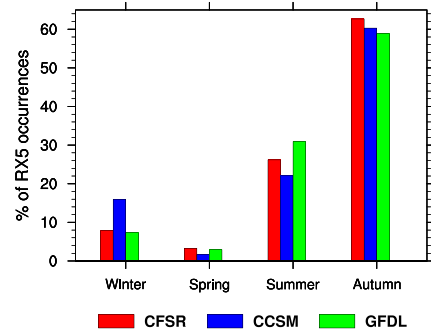
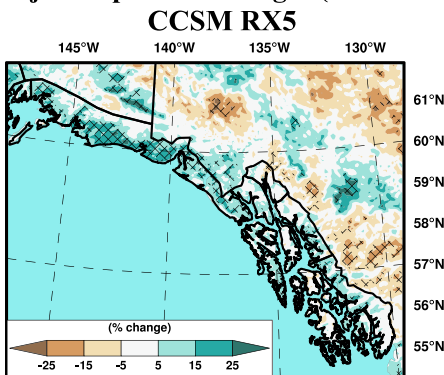
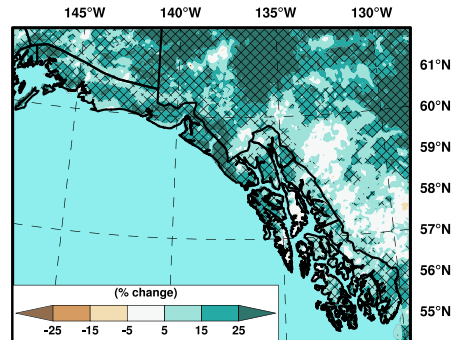
a) Climatological RX5**RX5 Seasonality****b) Projected percent changes (2031–2060 relative to 1981–2010)****GFDL RX5**

FIG. 6. As in Fig. 5, but for annual RX5 (cm).

single-day events to occur was in autumn (September–November), followed by summer (June–August), spring (March–May), and last, winter (December–February; see red bars in Fig. 5a, right). The CCSM showed a similar pattern, but the GFDL showed an RX1 peak occurring in the summer (blue and green bars in Fig. 5a, right, respectively). Projected RX1 amounts increased significantly by 12.6% in CCSM and 19.8% in GFDL across southeast Alaska (Table 2), and each division showed increases (Fig. 5b).

Figure 6a (left) depicts the historical CFSR RX5 climatology, showing extreme topographically based gradients. The southeast Alaska CFSR RX5 amount was 23.3 cm, which was lower than both the historical CCSM (28.1 cm) and GFDL (26.7 cm; Table 2). Unlike with RX1, where there was model disagreement as to the most likely season of occurrence, RX5 events in both models were likely to occur in autumn, followed by summer, winter and last, spring (Fig. 6a, right). The projected seasonality of RX5 and RX1 events did not change in either model in terms of which season ranked first through fourth. Both climate models projected significantly higher RX5 amounts, with CCSM (Fig. 6b, left) increasing by 7.4% and GFDL (Fig. 6b, right) increasing by 16.0% across southeast Alaska, and with each climate division indicating an increase (Table 2). These percent increases are lower than those projected for RX1 amounts, but higher than the annual projected precipitation increases of 6.2% by CCSM and 3.3% by GFDL (Table 1).

c. Snowfall indices

At all four stations the average number of days each year with SNC decreased significantly. A minimum of 95% daily data coverage was used as a threshold for inclusion for each year. The trend, measured in days per decade, was -4.9 at Yakutat (Fig. 7a), -4.7 at Juneau (Fig. 7b), -5.8 at Sitka (Fig. 7c), and -2.4 at Annette (Fig. 7d). The historical CFSR SNC climatology in Fig. 8a (left) showed an average across southeast Alaska of 192.1 days yr^{-1} (Table 3), which was considerably less than the historical CCSM (228.2 days yr^{-1}) and GFDL (227.0 days yr^{-1}). Recall that these values are averages over all grid cells in southeast Alaska, including glacial ones that have snow cover 365 days yr^{-1} , which is why they are substantially higher than those of the stations in Fig. 7. SNC days are projected to decrease significantly at nearly all locations, with an average loss of 21.4% in CCSM and 21.9% in GFDL (left side of Figs. 8b and 8c, respectively). The only grid cells that did not lose SNC days were the highest-elevation glacial ones that had snow cover every day in the historical and the future periods.

The regional CFSR SNF climatology showed considerable variability from rain dominant near the coast to snow dominant inland and at higher elevation (Fig. 8a, right). Consistent with how the historical climate models overestimated SNC days, they also had higher SNF values of 50.6% (CCSM) and 43.0% (GFDL) as compared with CFSR (33.6%; Table 3).

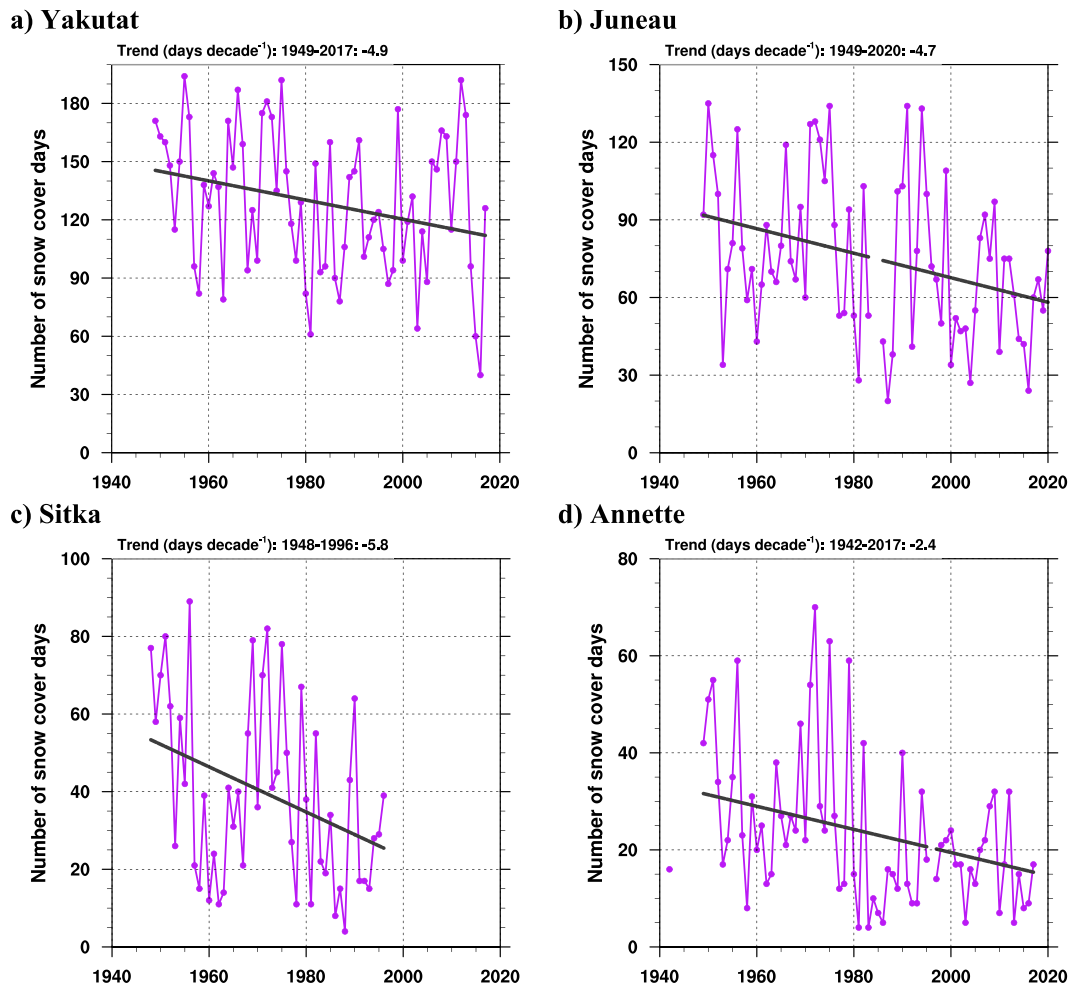


FIG. 7. Time series of the annual number of snow cover days (snow depth ≥ 2.54 cm) at (a) Yakutat, (b) Juneau, (c) Sitka, and (d) Annette. Theil-Sen trends of the full period of record are shown, with the values above each plot. A threshold of 95% daily data coverage was required for inclusion for each year.

Projected SNF changes from CCSM and GFDL (right-hand side of Figs. 8b,c) showed consistent significant decreases in snowfall relative to total annual precipitation. The average projected change across southeast Alaska was -24.4% in CCSM and -26.5% in GFDL (Table 3). The positive historical climate model SNF biases make sense given that each model was colder than the CFSR during autumn and winter. The most pronounced SNF projected decreases were in the Central Panhandle and South Panhandle. Similar to projected changes to SNC, the only unchanged values were those at the highest elevations, which were glacially covered.

Given the projection of significantly fewer SNC days and a lower SNF in both climate models, it follows that annual snowfall is also expected to decrease, however, there were a few locations with projected increases. Projected percent change maps of annual snowfall, measured as snow water equivalent, are shown in Fig. 9a for CCSM (left) and GFDL (right), and they indicate substantial snowfall loss, particularly in the Central and South Panhandle divisions where losses

often exceeded 50%. At the highest elevations, both climate models indicated areas with relatively little change or even increasing values; in CCSM this corresponded to locations above 1500 m and in GFDL this level is higher around 2500 m (Fig. 9b, left and right, respectively). The scatterplot in Fig. 9b also effectively shows the topographical distribution of southeast Alaska, with most grid cells below 1000 m. In CCSM 4.8% of grid cells projected increased snowfall and in GFDL only 0.1% did.

4. Discussion

Annual precipitation has been increasing across southeast Alaska and this trend is expected to continue, but there are multiple pathways as to how these increased amounts could occur. One pathway could result from lower variability and slightly higher intensity where every year generally gets wetter; but another pathway to overall wetter conditions could result from both higher variability and higher intensity, similar to

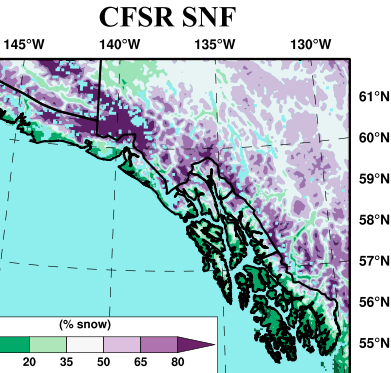
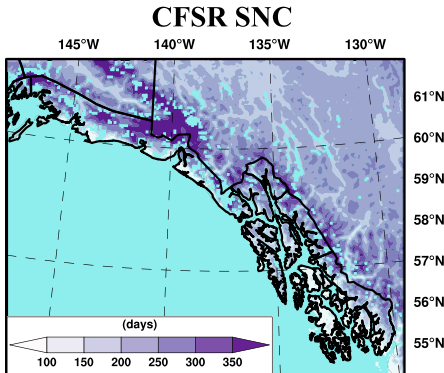
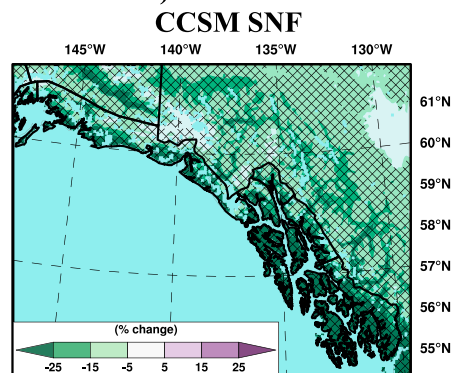
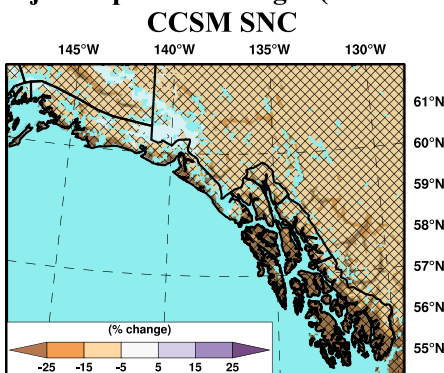
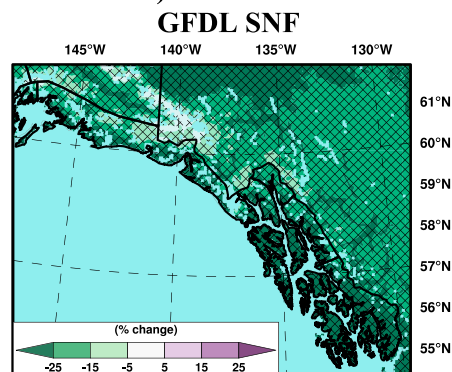
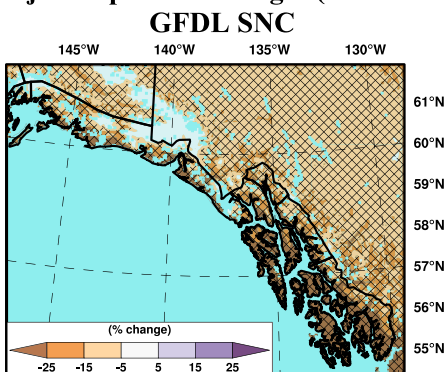
a) CFSR climatology (1981-2010)**b) Projected percent changes (2031-2060 relative to 1981-2010)****c) Projected percent changes (2031-2060 relative to 1981-2010)**

FIG. 8. As in Fig. 4, but for annual (left) SNC (days) and (right) SNF (%).

what occurred in southeast Alaska from 2019 to 2020. The model results are in good agreement that RX1 and RX5 amounts will increase, which supports the tendency toward higher intensities driving the total precipitation increase. As the time period of measurement for the hydroclimatic extremes indices decreases, the projected percent increase rises. CCSM shows projected increases of total annual precipitation, RX5, and RX1 of 6.2%, 7.4%, and 12.6%, respectively; GFDL similarly also shows higher increases for RX5 than for RX1, with corresponding changes of 3.3%, 16.0%, and 19.8%, respectively. All of these values except for the GFDL total annual precipitation increase were statistically significant. The RX1 and RX5 events typically occur in the autumn and are often

associated with ARs, as was the case with the 1 December 2020 event. Using a 21-member ensemble from CMIP5 RCP8.5, Espinoza et al. (2018) found a projected 6–percentage point increase (e.g., from 10%–12% to 16%–18%) in the frequency of time steps with an AR present and a projected integrated water vapor transport increase of $70 \text{ kg m}^{-2} \text{ s}^{-1}$ in the North Pacific when comparing 2073–96 with 1979–2002. These changes are consistent with a projected strengthening of the Aleutian low (Gan et al. 2017), which is strongest during the late-autumn and winter, and thus would transport moisture-laden air northward into southeast Alaska from the extratropics.

These findings suggest that outside of higher magnitude precipitation events, there must be more extended dry periods to

TABLE 3. Historical mean (1981–2010) and projected percent changes (2031–60) of annual snowfall in liquid equivalent (ACSNOW), annual number of snow cover days (SNC), and annual percentage of precipitation as snow (SNF) by model and climate division. Significant changes at 95% confidence are in boldface font.

Climate division	1981–2010 mean (cm; days; %)			2031–60 projected change ($\pm\%$)	
	CFSR	CCSM	GFDL	CCSM	GFDL
ACSNOW					
Northeast Gulf	142.8	237.4	226.3	-13.8	-21.3
North Panhandle	120.2	161.4	162.9	-13.0	-20.5
Central Panhandle	118.9	188.2	166.6	-19.8	-25.5
South Panhandle	64.7	108.4	90.6	-29.3	-31.2
Southeast Alaska	114.1	187.0	173.1	-17.4	-23.4
Annual no. of SNC					
Northeast Gulf	224.5	265.1	265.1	-17.5	-18.4
North Panhandle	256.7	273.7	289.4	-13.6	-15.8
Central Panhandle	207.8	239.1	244.1	-22.1	-23.2
South Panhandle	123.3	157.0	148.6	-33.7	-33.2
Southeast Alaska	192.1	228.2	227.0	-21.4	-21.9
Annual SNF					
Northeast Gulf	41.9	60.0	52.6	-20.9	-23.0
North Panhandle	52.9	69.7	62.4	-17.9	-22.2
Central Panhandle	33.6	51.0	43.2	-25.6	-29.1
South Panhandle	17.2	32.2	24.4	-36.5	-38.7
Southeast Alaska	33.6	50.6	43.0	-24.4	-26.5

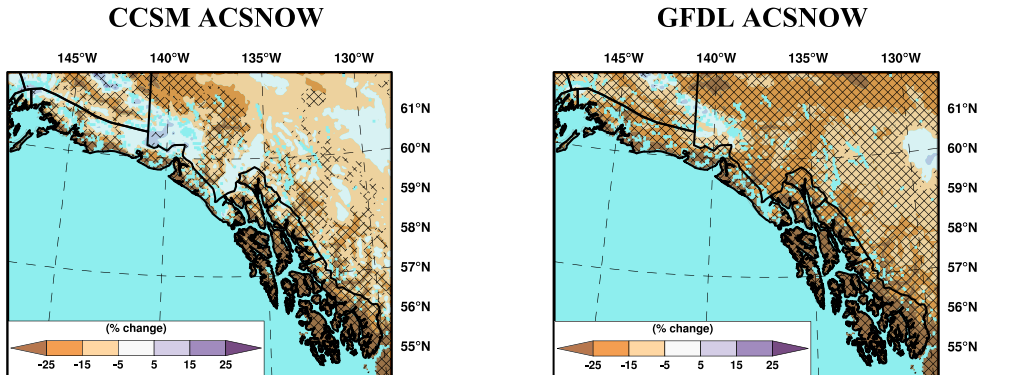
account for lower annual increases. This is supported by both the CCSM and GFDL CDD projections where the average southeast Alaska CDD value increases by 11.9% and 20.1%, respectively, with the latter being significant. Lader et al. (2020) found that the projected annual precipitation increases occurred due to higher autumn and winter amounts, but relatively little change or even slightly decreased spring and summer amounts; meanwhile, temperatures increased by 1°–3°C in all seasons. Historically, late winter into early spring was the most likely period for the annual CDD to occur and that remains true in the mid-century period; however, the likelihood of a summer CDD occurrence increases from 16.6% to 20.6% in CCSM and from 12.1% to 13.1% in GFDL. Collectively, then, with the results from this study, these projections suggest a heightened risk of short-term drought, particularly during warm summers. The term “flash drought” is regularly used to describe this type of rapid-onset hazard that can result from precipitation deficit and higher temperatures, although there is broad discussion about the specific criteria required and appropriate use of the term (Lisonbee et al. 2021; Otkin et al. 2018). The models disagreed on projections of CWD with CCSM having a 3.7% increase and GFDL showing a 7.0% decrease.

The human impacts of amplified hydroclimate extremes in southeast Alaska, both dry and wet, could be substantial, given the region’s dependence on hydropower for electricity. In 2013, over 99% of electricity generation came from hydropower at Juneau and 96% at Ketchikan (Alaska Energy Data Gateway 2021). With such reliance on hydropower, many communities were forced to transition to use of more-expensive diesel fuel to generate electricity during the summer drought of 2019 when reservoirs were critically low (Bathke et al.

2019). Increased extreme precipitation events, however, would not necessarily aid summer drought because the RX5 index is likely to occur in the autumn (Fig. 6a, right). It is possible that excess precipitation, relative to the historical period, could spillover already full reservoirs during the wet season and be lost. Furthermore, the models showed consistent results that snow cover days and snow fractions are projected to decrease (Figs. 8b,c) and annual snowfall-water equivalent decrease at all but the highest elevations (Fig. 9). With regard to the snow indices, much of southeast Alaska historically had temperatures near or just below freezing during the cold months of the year, meaning that a projected warming of 1°–3°C would likely be the main factor explaining trends of snow cover loss and snowfall decrease. This would suggest an increase in winter runoff and this water would not be stored on the landscape, and only be available to help replenish reservoir levels in the spring and summer if not already full.

Ecologically, the projected changes in hydroclimatic extremes toward more intense precipitation events, longer dry periods, and substantially lower snow fractions—all a response to increasingly warmer temperatures—pose challenges to the Pacific salmon populations of southeast Alaska. Many salmon species in this region have been declining in average size while tending to mature earlier since the dramatic change toward warmer sea surface temperatures associated with the 1976/77 Pacific decadal oscillation shift (Lewis et al. 2015). Warmer sea surface temperatures and increased precipitation have been found to correspond to earlier salmon migration (Kovach et al. 2015). More extreme precipitation events, which predominantly occur in the autumn (e.g., RX5) during spawning, increase the risk of salmon egg mortality from landslide scour

a) Projected percent changes (2031–2060 relative to 1981–2010)



b) Projected percent changes by elevation

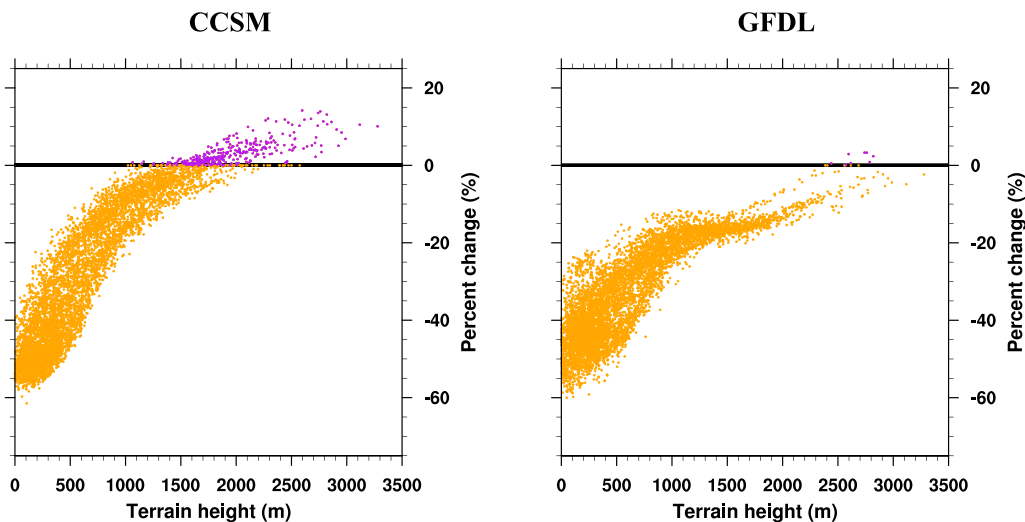


FIG. 9. (a) Projected percent changes in ACSNOW (cm; 2031–60 mean relative to 1981–2010 mean) from the down-scaled 4-km CCSM (left panel) and GFDL (right panel) and (b) by elevation for each land grid cell in Southeast Alaska from CCSM (left panel) and GFDL (right panel). Significant changes in (a) that met the 95% confidence level are hatched.

(Bryant 2009; Shanley and Albert 2014). However, while the projected climatic changes generally suggest harmful effects to Pacific salmon, the source of water for individual streams complicates these issues in southeast Alaska. Those that are glacially dominant have historically been cooled below an optimal temperature threshold by meltwater; thus, as snowfall decreases and glaciers recede, these watersheds could have enhanced productivity (Fellman et al. 2014).

The results in this study were derived from downscaled simulations of two models based on the RCP8.5 emissions scenario from CMIP5. These two models were selected based on their strong performances in simulating air temperature, precipitation, and sea level pressure in Alaska (Walsh et al. 2018) and because they provided a range of climate sensitivity to changing emissions with CCSM being less sensitive and GFDL more sensitive (Flato et al. 2013). CMIP6 has recently become available, and one of its goals is to better understand “the factors that control water availability over land” (Eyring

et al. 2016). CMIP6 uses a new set of five Shared Socioeconomic Pathways that include changes to radiative forcing, as with the RCPs, but now include a broader range of policy assumptions, land-use changes, and technological development (Riahi et al. 2017). A set of eight CMIP6 models projected lower midcentury increases in total precipitation and shorter CDD periods than CMIP5 for an Alaska domain; however, the southern half of southeast Alaska was not included (Li et al. 2021). Southeast Alaska is a region with steep topographical gradients and rapidly varying landscapes; thus, future research on hydroclimatic extremes that is directly focused on this region could benefit by investigating these next generation climate simulations.

5. Summary

Recent hydroclimatic extremes in southeast Alaska have posed challenges to the region’s energy infrastructure, its

culturally significant and economically important fisheries, and basic necessities like municipal water supply. The drought that peaked in summer 2019 was followed by record-setting daily precipitation in late 2020. The observational trends analyzed in this study did not support a directional change toward higher or lower annual precipitation variability; however, such projected changes were found at the daily and subseasonal scale. Consistent midcentury 4-km downscaled projections (RCP8.5; 2031–60), relative to the historical climate (1981–2010), were found from both CCSM4 and GFDL CM3 for annual-based values of maximum 1-day (RX1; higher) and 5-day (RX5; higher) precipitation, maximum number of consecutive dry days (CDD; longer), snow cover days (SNC; fewer), and snow fraction of total precipitation (SNF; lower), but not for maximum number of consecutive wet days (CWD). These findings can help to inform discussion concerning increased risk of flooding, landslides, avalanche exposure, short-term drought, and ecological impacts in southeast Alaska.

Acknowledgments. This research was funded by the U.S. Geological Survey Alaska Climate Adaptation Science Center. The project described in this publication was supported by Grant G21AC10110 from the U.S. Geological Survey. The views and conclusions contained in this document are those of the authors and should not be interpreted as representing the opinions or policies of the U.S. Geological Survey. Mention of trade names or commercial products does not constitute their endorsement by the Alaska Climate Adaptation Science Center or the U.S. Geological Survey. This paper was submitted for publication with the understanding that the U.S. government is authorized to reproduce and distribute reprints for governmental purposes.

Data availability statement. The authors confirm that all data used in this study are publicly available. The daily and monthly station data used in this study are available from the Global Historical Climatology Network–Daily database (<https://www.ncdc.noaa.gov/products/land-based-station/global-historical-climatology-network-daily>) and the NOAA NCEI Climate at a Glance tool (<https://www.ncdc.noaa.gov/cag/>), respectively. The dynamically downscaled reanalysis and climate model simulations are available from the Scenarios Network for Alaska and Arctic Planning (<https://registry.opendata.aws/wrf-se-alaska-snap/>).

REFERENCES

- Alaska Energy Data Gateway, 2021: Community data summaries. Accessed 1 November 2021, <https://iseralaska.org/projects/aedg/>.
- Anchorage Daily News, 2020: In photos: Haines grapples with landslides and flooding after a record-breaking storm. *Anchorage Daily News*, 4 December, <https://www.adn.com/visual/photos/2020/12/04/in-photos-haines-grapples-with-landslides-and-flooding-after-a-record-breaking-storm/>.
- Bathke, D. J., H. R. Prendeville, A. Jacobs, R. Heim, R. Thoman, and B. Fuchs, 2019: Defining drought in a temperate rainforest. *Bull. Amer. Meteor. Soc.*, **100**, 2665–2668, <https://doi.org/10.1175/BAMS-D-19-0223.1>.
- Bieniek, P. A., and Coauthors, 2012: Climate divisions for Alaska based on objective methods. *J. Appl. Meteor. Climatol.*, **51**, 1276–1289, <https://doi.org/10.1175/JAMC-D-11-0168.1>.
- Bryant, M. D., 2009: Global climate change and potential effects on Pacific salmonids in freshwater ecosystems of southeast Alaska. *Climatic Change*, **95**, 169–193, <https://doi.org/10.1007/s10584-008-9530-x>.
- Dettinger, M., 2005: Changes in streamflow timing in the western United States in recent decades. USGS Fact Sheet 2005-3018, 4 pp., https://pubs.usgs.gov/fs/2005/3018/pdf/FS2005_3018.pdf.
- , 2013: Atmospheric rivers as drought busters on the U.S. West Coast. *J. Hydrometeor.*, **14**, 1721–1732, <https://doi.org/10.1175/JHM-D-13-02.1>.
- Donner, L. J., and Coauthors, 2011: The dynamical core, physical parameterizations, and basic simulation characteristics of the atmospheric component AM3 of the GFDL global coupled model CM3. *J. Climate*, **24**, 3484–3519, <https://doi.org/10.1175/2011JCLI3955.1>.
- Easterling, D. R., and Coauthors, 2017: Precipitation change in the United States. *Climate Science Special Report: Fourth National Climate Assessment*, D. J. Wuebbles et al., Eds., Vol. I, U.S. Global Change Research Program, 207–230, <https://doi.org/10.7930/J0H993CC>.
- EPA, 2017: Climate impacts on energy. U.S. Environmental Protection Agency, accessed 18 August 2021, <https://19january2017snapshot.epa.gov/climate-impacts/climate-impacts-energy.html>.
- Espinoza, V., D. E. Waliser, B. Guan, D. A. Lavers, and F. M. Ralph, 2018: Global analysis of climate change projection effects on atmospheric rivers. *Geophys. Res. Lett.*, **45**, 4299–4308, <https://doi.org/10.1029/2017GL076968>.
- Eyring, V., S. Bony, G. A. Meehl, C. A. Senior, B. Stevens, R. J. Stouffer, and K. E. Taylor, 2016: Overview of the Coupled Model Intercomparison Project phase 6 (CMIP6) experimental design and organization. *Geosci. Model Dev.*, **9**, 1937–1958, <https://doi.org/10.5194/gmd-9-1937-2016>.
- Fellman, J. B., S. Nagorski, S. Pyare, A. W. Vermilyea, D. Scott, and E. Hood, 2014: Stream temperature response to variable glacier coverage in coastal watersheds of southeast Alaska. *Hydrolog. Processes*, **28**, 2062–2073, <https://doi.org/10.1002/hyp.9742>.
- Flato, G., and Coauthors, 2013: Evaluation of climate models. *Climate Change 2013: The Physical Basis*, T. F. Stocker et al., Eds., Cambridge University Press, 741–882, <https://doi.org/10.1017/CBO9781107415324.020>.
- Gan, B., L. Wu, F. Jia, S. Li, W. Cai, H. Nakamura, M. A. Alexander, and A. J. Miller, 2017: On the response of the Aleutian Low to greenhouse warming. *J. Climate*, **30**, 3907–3925, <https://doi.org/10.1175/JCLI-D-15-0789.1>.
- Gent, P. R., and Coauthors, 2011: The Community Climate System Model version 4. *J. Climate*, **24**, 4973–4991, <https://doi.org/10.1175/2011JCLI4083.1>.
- Gershunov, A., and Coauthors, 2019: Precipitation regime change in western North America: The role of atmospheric rivers. *Sci. Rep.*, **9**, 9944, <https://doi.org/10.1038/s41598-019-46169-w>.
- Gu, H., J. Jin, Y. Wu, M. B. Ek, and Z. M. Subin, 2015: Calibration and validation of lake surface temperature simulations with the coupled WRF-Lake model. *Climatic Change*, **129**, 471–483, <https://doi.org/10.1007/s10584-013-0978-y>.
- Hong, S.-Y., Y. Noh, and J. Dudhia, 2006: A new vertical diffusion package with an explicit treatment of entrainment processes. *Mon. Wea. Rev.*, **134**, 2318–2341, <https://doi.org/10.1175/MWR3199.1>.

- Iacono, M. J., J. S. Delamere, E. J. Mlawer, M. W. Shepard, S. A. Clough, and W. D. Collins, 2008: Radiative forcing by long-lived greenhouse gases: Calculations with the AER radiative transfer models. *J. Geophys. Res.*, **113**, D13103, <https://doi.org/10.1029/2008JD009944>.
- IPCC, 2012: Summary for policymakers. *Managing the Risks of Extreme Events and Disasters to Advance Climate Change Adaptation*, C. B. Field et al., Eds., Cambridge University Press, 1–19.
- Jiménez, P. A., J. Dudhia, J. F. González-Rouco, J. Navarro, J. P. Montávaz, and E. García-Bustamante, 2012: A revised scheme for the WRF surface layer formulation. *Mon. Wea. Rev.*, **140**, 898–918, <https://doi.org/10.1175/MWR-D-11-00056.1>.
- Knowles, N., M. D. Dettinger, and D. R. Cayan, 2006: Trends in snowfall versus rainfall in the western United States. *J. Climate*, **19**, 4545–4559, <https://doi.org/10.1175/JCLI3850.1>.
- Kovach, R. P., S. C. Ellison, S. Pyare, and D. A. Tallmon, 2015: Temporal patterns in adult salmon migration timing across southeast Alaska. *Global Change Biol.*, **21**, 1821–1833, <https://doi.org/10.1111/gcb.12829>.
- Lader, R., U. S. Bhatt, J. E. Walsh, T. S. Rupp, and P. A. Bieniek, 2016: Two-meter temperature and precipitation from atmospheric reanalysis evaluated for Alaska. *J. Appl. Meteor. Climatol.*, **55**, 901–922, <https://doi.org/10.1175/JAMC-D-15-0162.1>.
- , A. Bidlack, J. E. Walsh, U. S. Bhatt, and P. A. Bieniek, 2020: Dynamical downscaling for southeast Alaska: Historical climate and future projections. *J. Appl. Meteor. Climatol.*, **59**, 1607–1623, <https://doi.org/10.1175/JAMC-D-20-0076.1>.
- Lewis, B., W. S. Grant, R. E. Brenner, and T. Hamazaki, 2015: Changes in size and age of Chinook salmon *Oncorhynchus tshawytscha* returning to Alaska. *PLOS ONE*, **10**, e0130184, <https://doi.org/10.1371/journal.pone.0130184>.
- Li, J., R. Huo, H. Chen, Y. Zhao, and T. Zhao, 2021: Comparative assessment and future prediction using CMIP6 and CMIP5 for annual precipitation and extreme precipitation simulation. *Front. Earth Sci.*, **9**, 687976, <https://doi.org/10.3389/feart.2021.687976>.
- Lindsay, R., M. Wensnahan, A. Schweiger, and J. Zhang, 2014: Evaluation of seven different atmospheric reanalysis products in the Arctic. *J. Climate*, **27**, 2588–2606, <https://doi.org/10.1175/JCLI-D-13-00014.1>.
- Lisonbee, J., M. Woloszyn, and M. Skumanich, 2021: Making sense of flash drought: Definitions, indicators, and where we go from here. *J. Appl. Serv. Climatol.*, **2021**, 1–19, <https://doi.org/10.46275/JOASC.2021.02.001>.
- Mann, H. B., and D. R. Whitney, 1947: On a test of whether one of two random variables is stochastically larger than the other. *Ann. Math. Stat.*, **18**, 50–60, <https://doi.org/10.1214/aoms/1177730491>.
- Menne, M. J., I. Durre, R. S. Vose, B. E. Gleason, and T. G. Houston, 2012: An overview of the Global Historical Climatology Network-Daily database. *J. Atmos. Oceanic Technol.*, **29**, 897–910, <https://doi.org/10.1175/JTECH-D-11-0013.1>.
- Monaghan, A. J., M. P. Clark, M. P. Barlage, A. J. Newman, L. Xue, J. R. Arnold, and R. M. Rasmussen, 2018: High-resolution historical climate simulations over Alaska. *J. Appl. Meteor. Climatol.*, **57**, 709–731, <https://doi.org/10.1175/JAMC-D-17-0161.1>.
- National Drought Mitigation Center, 2021: U.S. Drought Monitor. Accessed 27 October 2021, <https://droughtmonitor.unl.edu>.
- NCAR, 2022: NCAR Command Language Version 6.4.0. UCAR/NCAR/CISL/TDD, <https://doi.org/10.5065/D6WD3XH5>.
- Niu, G.-Y., and Coauthors, 2011: The community Noah land surface model with multiparameterization options (Noah-MP): 1. Model description and evaluation with local-scale measurements. *J. Geophys. Res.*, **116**, D12109, <https://doi.org/10.1029/2010JD015139>.
- NOAA NCEI, 2015: State of the Climate—National climate report for February 2015: Alaska Climate Divisions FAQ's. Accessed 30 October 2021, <https://www.ncei.noaa.gov/access/monitoring/monthly-report/national/201502/supplemental/page-5>.
- , 2021: Climate at a Glance: Divisional time series. Accessed 28 October 2021, <https://www.ncdc.noaa.gov/cag>.
- Otkin, J. A., M. Svoboda, E. D. Hunt, T. W. Ford, M. C. Anderson, C. Hain, and J. B. Basara, 2018: Flash droughts: A review and assessment of the challenges imposed by rapid-onset droughts in the United States. *Bull. Amer. Meteor. Soc.*, **99**, 911–919, <https://doi.org/10.1175/BAMS-D-17-0149.1>.
- Prein, A. F., and Coauthors, 2015: A review of regional convection-permitting climate modeling: Demonstrations, prospects, and challenges. *Rev. Geophys.*, **53**, 323–361, <https://doi.org/10.1002/2014RG000475>.
- R Core Team, 2022: R: A Language and Environment for Statistical Computing. R Foundation for Statistical Computing, <https://www.R-project.org/>.
- Riahi, K., and Coauthors, 2011: RCP 8.5—A scenario of comparatively high greenhouse gas emissions. *Climatic Change*, **109**, 33, <https://doi.org/10.1007/s10584-011-0149-y>.
- , and Coauthors, 2017: The Shared Socioeconomic Pathways and their energy, land use, and greenhouse gas emissions implications: An overview. *Global Environ. Change*, **42**, 153–168, <https://doi.org/10.1016/j.gloenvcha.2016.05.009>.
- Saha, S., and Coauthors, 2010: The NCEP Climate Forecast System Reanalysis. *Bull. Amer. Meteor. Soc.*, **91**, 1015–1058, <https://doi.org/10.1175/2010BAMS3001.1>.
- Sen, P. K., 1968: Estimates of the regression coefficient based on Kendall's tau. *J. Amer. Stat. Assoc.*, **63**, 1379–1389, <https://doi.org/10.1080/01621459.1968.10480934>.
- Shanley, C. S., and D. M. Albert, 2014: Climate change sensitivity index for Pacific salmon habitat in southeast Alaska. *PLOS ONE*, **9**, e104799, <https://doi.org/10.1371/journal.pone.0104799>.
- Sharma, A. R., and S. J. Déry, 2020: Contribution of atmospheric rivers to annual, seasonal, and extreme precipitation across British Columbia and southeastern Alaska. *J. Geophys. Res. Atmos.*, **125**, e2019JD031823, <https://doi.org/10.1029/2019JD031823>.
- Skamarock, W. C., and Coauthors, 2019: A description of the Advanced Research WRF Model version 4. NCAR Tech. Note NCAR/TN-556+STR, 145 pp, <https://doi.org/10.5065/1dfh-6p97>.
- Stewart, I. T., 2009: Changes in snowpack and snowmelt runoff for key mountain regions. *Hydrol. Processes*, **23**, 78–94, <https://doi.org/10.1002/hyp.7128>.
- Subin, Z. M., W. J. Riley, and D. Mironov, 2012: An improved lake model for climate simulations: Model structure, evaluation, and sensitivity analyses in CESM1. *J. Adv. Model. Earth Syst.*, **4**, M02001, <https://doi.org/10.1029/2011MS000072>.
- Taylor, K. E., R. J. Stouffer, and G. A. Meehl, 2012: An overview of CMIP5 and the experiment design. *Bull. Amer. Meteor. Soc.*, **93**, 485–498, <https://doi.org/10.1175/BAMS-D-11-00094.1>.
- Theil, H., 1950: A rank-invariant method of linear and polynomial regression analysis. *Proc. K. Ned. Akad. Wet.*, **53A**, 386–392.
- Thoman, R., and J. E. Walsh, 2019: Alaska's changing environment: Documenting Alaska's physical and biological changes through observations. International Arctic Research Center

- Doc., 15 pp., <https://uaf-iarc.org/our-work/alaskas-changing-environment/>.
- Thompson, G., P. R. Field, R. M. Rasmussen, and W. D. Hall, 2008: Explicit forecasts of winter precipitation using an improved bulk microphysics scheme. Part II: Implementation of a new snow parameterization. *Mon. Wea. Rev.*, **136**, 5095–5115, <https://doi.org/10.1175/2008MWR2387.1>.
- Vahedifard, F., J. D. Robinson, and A. AghaKouchak, 2016: Can protracted drought undermine the structural integrity of California's earthen levees? *J. Geotech. Geoenviron. Eng.*, **142**, 02516001, [https://doi.org/10.1061/\(ASCE\)GT.1943-5606.0001465](https://doi.org/10.1061/(ASCE)GT.1943-5606.0001465).
- Vose, R., and Coauthors, 2017: Deriving historical temperature and precipitation time series for Alaska climate divisions via climatologically aided interpolation. *J. Appl. Serv. Climatol.*, **10**, 1–20, <https://doi.org/10.46275/JoASC.2017.10.001>.
- Walsh, J. E., and Coauthors, 2014: Our changing climate. *Climate Change Impacts in the United States: The Third National Climate Assessment*, J. M. Melillo, T. C. Richmond, and G. W. Yohe, Eds., U.S. Global Change Research Program, 19–67, <https://doi.org/10.7930/J0Z31WJ2>.
- , and Coauthors, 2018: Downscaling of climate model output for Alaskan stakeholders. *Environ. Modell. Software*, **110**, 38–51, <https://doi.org/10.1016/j.envsoft.2018.03.021>.
- Wehner, M. F., J. R. Arnold, T. Knutson, K. E. Kunkel, and A. N. LeGrande, 2017: Droughts, floods, and wildfires. *Climate Science Special Report: Fourth National Climate Assessment*, D. J. Wuebbles et al., Eds., Vol. I, U.S. Global Change Research Program, 231–256, <https://doi.org/10.7930/J0CJ8BNN>.
- Zhang, X., L. Alexander, G. C. Hegerl, P. Jones, A. Klein Tank, T. C. Peterson, B. Trewin, and F. W. Zwiers, 2011: Indices for monitoring changes in extremes based on daily temperature and precipitation data. *Wiley Interdiscip. Rev.: Climate Change*, **2**, 851–870, <https://doi.org/10.1002/wcc.147>.